The published version of the paper "Ivan Navarro-Baena, Valentina Sessini, Franco Dominici, Luigi Torre, Jose M. Kenny, Laura Peponi, Design of biodegradable blends based on PLA and PCL: From morphological, thermal and mechanical studies to shape memory behavior, Polymer Degradation and Stability, 132, 97-108" is available at: https://doi.org/10.1016/j.polymdegradstab.2016.03.037

Design of biodegradable blends based on PLA and PCL: From morphological, thermal and mechanical studies to shape memory behavior

Ivan Navarro-Baena [a], Valentina Sessini [a], Franco Dominici [a], Luigi Torre [a],

Jose M. Kenny [a, b], Laura Peponi [b, *]

[a] *Dipartimento di Ingegneria Civile e Ambientale, Università di Perugia, Italy*

[b] *Instituto de Ciencia y Tecnología de Polímeros, ICTP-CSIC, Spain*

Abstract

Blending commercial homopolymers represents a low cost and an easy scalable process to extend the use of the pristine homopolymers to an industrial level. Actually, the processing of blends by extrusion is the usual solution followed in the industry. However, commonly polymer blends are immiscible, provoking phase separation, which can be in the macro, micro or nano scale, depending on the polymers as well as on the processing conditions, affecting the final properties of the blends. Therefore, this paper aims to study the shape memory behavior in biodegradable blends based on poly(lactic acid) (PLA) and poly(ε-caprolactone) (PCL) in different concentrations. A completely thermal and mechanical characterization of the blends was performed, correlating the results with the observed morphology. In addition, two different biodegradation studies were performed in order to correlate the effect of each homopolymer with the degradation behavior of the biodegradable blends.

1. Introduction

The growing interest on new materials for advanced fields such as biomedicine or packaging applications have increased the attention on biodegradable polymer blends in recent years [1-4]. In general, the processing of polymer blends is an interesting goal for both research groups and industrial companies because of it is an easy, low-cost, scalable way to enhance the properties of the pristine homopolymers [5,6]. The most commercial polymer blends are immiscible, thus presenting two separated phase. However, still in this case, they have very useful properties [7]. Depending on the thermodynamics of the system, the processing conditions and the composition of the blends, they can present phase separation thus forming morphological structures, such as spherical droplet, elongated or fibrous structure and co-continuous structure [8,9]. The final properties of the blends are strongly affected by the phase separated morphology,

and thus controlling this morphology it is possible to take advantage of the homopolymer synergetic effects improving the final properties of the blend [10,11]. In this context, blends of PLA with other aliphatic polyesters, in particular with poly(ε-caprolactone) (PCL), have attracted the attention of many research groups [12e16], due to the fact that both polymers are biodegradable and biocompatible [17e22] with attractive synergic properties, referring to their thermal behavior, mechanical [23] and rheological properties [9,24,25] or biodegradation rates [19,26]. Moreover, another interesting property to study when working with PLA- and PCL-based materials is the shape memory effect [27,28]. This particular behavior consists in the ability of the material to change its initial shape by the application of certain external stimulus, usually the temperature [29], and to recover its initial shape when the external stimulus is applied again. Generally, shape memory behavior is achieved by designing materials with two or more phases, where one is responsible to fix the original shape, while the other one enables the modeling of the desired temporary shape [28]. Therefore, the shape memory process comprises two stages known as programming and recovery. In particular, during the programming process, a temporary shape is fixed from the original shape, while during the recovery process the fixed shape is recovered from the temporary one [30]. Moreover, when the external stimulus responsible for the shape change is the temperature, the recovery consists of heating the material above its transition temperature, generally the melting temperature (Tm) or the glass transition temperature (Tg) of the temporary phase [28]. Different materials based on PLA have been studied for shape memory applications [31]. For instance, Peponi et al. studied polyurethanes based on tri-block copolymers of PCL and poly(Llactic acid) (PLLA) with shape memory behavior [32] as well as their nanocomposites reinforced with cellulose nanocrystals, with a transition temperature close to the body temperature [29]. Several studies have been reported to improve the miscibility of PCL and PLA blend [10,23,33,34]. Lopez-Rodriguez et al. studied blends of PLLA and poly(D-Lactic acid) (PDLA) with PCL at different ratios in terms of crystallization, morphology and mechanical properties [24]. Chen et al. blended PLA and PCL in solution, and they added a copolymer of poly(ethylene oxide) and poly(- propylene oxide) as compatibilizer to enhance the mechanical properties with the aim of getting a material tougher than the pristine PLLA. Other way to enhance the miscibility is obtained by using amphiphilic copolymers as compatibilizers [35], incorporating some additives [36] or controlling the processing conditions [37]. Moreover, the interest of new ternary blends has also been increased in the last years in order to obtain a final material at low costs with better properties. Carmona et al. studied ternary blends of PCL/PLA and thermoplastic starch (TPS) prepared by extrusion, adding different compatibilizing agents in order to improve their final properties [22,36]. Gardella et al. studied PLA grafted with maleic acid in order to compatibilize the PLA/PCL blend with 70 wt % of PLA reporting changes in the morphology, in the thermal behavior as well as an improvement in the elongation at break [38]. Also the addition of nanoparticles [11,39-42], such as polyhedral oligomeric silsesquioxanes (POSS) has been reported to improve the miscibility of PLA/PCL blend [43]. In this paper the attention has been focused on the design of PLA and PCL biodegradable blends with shape memory properties. In particular, a series of PLA/PCL blends has been obtained by the variation of the mass fraction across the composition range, obtaining a wide range of mechanical response. Their nanocharacterization, in terms of morphology and physico-chemical properties has been used in order to

understand their behavior at macro-scale level. Moreover, due to their potential applications in the field of biomedicine as well as in the food packaging or agriculture, two degradation analyses were performed for the PLA/PCL blends, that is, the in vitro degradation with phosphate buffer solution (PBS) and the degradation under compost conditions at lab scale. Therefore, this work demonstrates the possibility to obtain multifunctional blends by a low-cost and an easy industrial-scale process, for applying in several innovative fields where biodegradable polymers are required such as biomedicine, food packaging and agriculture among others.

2. Materials and methods

2.1. Materials

PLA grade 3051D was supplied by NatureWorks® while PCL CAPA8000 was kindly donated by Perstop. All the blends were processed by extrusion using a DSM Xplore co-rotating extruder at a screw speed of 100 rpm. Prior to melt-blending the polymers were dried in a vacuum oven at 40 C during 24 h. Ten grams of material were added and to ensure the fully filling of the extruder, pre-mixture was added until the measured normal force was kept at 3000-3500 N. The mixing time was kept constant in all cases and equal to 3 min. The profile temperature in the screws was selected to obtain a melt temperature of 180 C inside the extruder. After the extrusion process, the material was compressed moulded into films of 500 mm by using a Dr. Collin 200 200 hot plate press at 180 °C. First the samples were heated during 1 min at atmospheric pressure and then 50 bar of pressure were applied during 1 min. The obtained films were cooled to room temperature with water-refrigerated aluminium plates at 50 bar. The three blends are named MxPLA, where x corresponds to the percentage of PLA in the blend such as M70PLA, M50PLA and M30PLA. At the same time, M100PLA and M0PLA correspond to the neat PLA and the neat PCL, respectively have been processed.

2.2. Characterization techniques

The morphology of the blends was investigated by Field Emission Scanning Electron Microscopy (FE-SEM Supra 25, Zeiss), and by RAMAN spectroscopy. For the FE-SEM characterization all the samples were gold coated by an Agar automatic sputter coated. On the other hand, Raman spectra mapping is a method for generating detailed chemical images based on a Raman spectrum of the sample. For Raman mapping measurement a Renishaw InVia Reflex Raman Microscope (Wotton-Under-Edge, UK) system was used. An optical microscope is coupled to the system. The laser beam is focused on the sample with an Olympus 0.75 - 50 microscope objective. The spatial resolutionwas about 1.22 mm. Calibration was done by referring to the 520 cmA1 line of silicon. The Raman scattering was excited using a diode laser at a wavelength of 785 nm (320mWpower). An automatic motorized translator X-Y stage was used to collect two dimensions images. A total of 960 spectra was recorded at the interval of 800 cmA1 and 1150 cmA1 in order to mapping the different areas, thus considering the vibration band of PLA at 873 cmA1 and the skeletal stretching for PCL at 1109 cm-1.

The thermal characterization was performed by dynamic Differential Scanning Calorimetry (DSC) analysis and by thermogravimetric analysis (TGA). For DSC measurements a Mettler Toledo DSC822e instrument was used. Thermal cycles was composed by three cycles: a first heating scan, from 25 °C to 200 °C, to erase the thermal history of the sample, a cooling scan from 200 °C to -90 °C and finally, another heating scan from -90 °C to 200 °C. The three scans were performed with a heating rate of 10 C/min run under nitrogen purge (30 mL/min). The degree of crystallinity (Xc) was determined by means of Eq. (1).

$$X_c = 100\% \cdot \left[\frac{\Delta H_m - \Delta H_{cc}}{\Delta H_{m0}}\right] \cdot \frac{1}{W} \quad (1)$$

where, DHm0 is the enthalpy value of a pure crystalline material, DHm is the enthalpy corresponding to the fusion process and W the amount of each homopolymer in the blend. The reference value taken for DHm0 of PCL was 148 kJ/mol, while for the PLA was 93 kJ/ mol [44].

The TGA measurements were carried out using a TA-TGA Q500 analyzer. The experiments were performed using about 10 mg of sample from room temperature to 700 C at 10 C/min under nitrogen atmosphere (60 mL/min). Fourier transform infrared (FT-IR) spectra were obtained in the attenuated total reflectance (ATR) mode. The measurements were performed using a Spectrum One FT-IR spectrometer Perkin Elmer equipped with an internal reflection element of diamond in the range of 650-4000 cm-1 with 1 cm-1 of resolution and an accumulation of 16 scans.

The molecular weight was investigated by means of Gel Permeation Chromatography (GPC) using a refractometer index detector Waters 2414. For the determination of molecular weight the samples were referenced to polystyrene standards between 4000 and 400.000 g/mol. The samples were prepared dissolving 5 mg of sample in 1 mL of filtered tetrahydrofuran (THF).

The mechanical properties were tested by using an Instron Universal Testing Machine at a strain rate of 200 mm/min with a load cell of 100 N. Measurements were performed on 5 dog-bone specimens with a width of 2 mm and leaving an initial length between the clamps of 20 mm. From these experiments were calculated the elastic modulus, as the slope of the curve between 0% and 2% of deformation, the elongation at break and the maximum tensile strain for each blend.

Dynamic mechanical analysis was performed on a Mettler Toledo 861e instrument at 1 Hz frequency in tensile configuration. The damping factor (tan d) and the storage modulus were measured from A120 C temperature to -20 °C at 1.5°C/min. Thermo-mechanical cycles were performed in order to study the shape memory behavior at a strain rate of 10 mm/min, at a deformation of 50% and at a transition temperature of 55 °C. The samples used for the shape memory analysis were cut from compression moulded thin films into rectangular samples with 20 mm in length and 5 mm in width. Samples were first heated up to the stretching temperature, 55 C, for 10 min. Then, a stress controlled uniaxial stretching was applied until reach 50% of strain. The stress is held constant during subsequent quenching to the fixing temperature, 15 °C, during 6 min and then the stress was removed, fixing the temporary shape. A free-strain recovery is

performed under continuous heating condition until 55 °C, thus recovering the initial shape. Two are the main parameters used to study the shape memory effect, the strain recovery ration Rr and the strain fixity ratio, Rf, following the equations:

$$R_f\ (N) = \frac{\varepsilon_u(N)}{\varepsilon_m} \cdot 100 \qquad (2)$$

$$R_r(N) = \frac{\varepsilon_m - \varepsilon_p(N)}{\varepsilon_m - \varepsilon_p(N-1)} \cdot 100 \qquad (3)$$

In particular, Rf indicates the ability of the material to fix the transient shape while Rr indicates their ability to recovery its initial shape.

The in vitro degradation tests under hydrolytic conditions were performing by immersing the samples at 37 °C and using a phosphate buffer solution (PBS), with a pH of about 7.2e7.4. The PBS was purchased by Sigma Aldrich. Each sample was immersed in a bottle of 15 mL, filled with 10 mL of solution. The PBS was changed once a week and the pH was checked after each week. The degradation tests under compost conditions were carried out following the ISO 20200 standard. The wt % of the components involved in the compost is summarized in Table 1. The experiments were performed in polypropylene vessels of 5 x 14 x22 cm. The samples were put at about middle height in the vessels, covered up and down with two net papers, which permit the contact of samples with the compost as well as to facilitate the recovering of the degraded samples after the experiments. Each vessel contained six samples. The experiments were performed during six weeks, using different samples for every week. All the vessels were introduced in an oven with ventilation at 58 °C, and all the days the weight of the vessels was measured. Their weight lost corresponds to the water evaporation, so they were re-filled with water in order to preserve the composting conditions.

3. Results and discussions

Phase separation is a key-factor to understand the macroscopic properties of polymeric blends. In Fig. 1, the FE-SEM images for the three blends at different magnifications are shown. All the blends present the phase separation characteristic of an immiscible polymeric blend. In particular, for M30PLA the formation of irregular PLA micrometer spheres with different dimension ranging from ten to one micron, immersed in the PCL continuous phase can be observed (Fig. 1c, f, i). On the other hand, the blend M50PLA presents co-continuous phases of each homopolymer, showing the presence of very few irregular spheres. However, big magnifications are needed to detect the phase-separated spheres. Finally in M70PLA the inversion of phase occurred and small PCL spheres can be detected thus indicating, little adhesion with PLA matrix, which confirms their strong incompatibility. Confocal RAMAN spectroscopy was used in order to confirm the phase separation in the different polymeric blends. In fact, this technique can be considered as a good

method to study both the phase separation and the distribution of the homopolymers in the polymer blends, allowing the identification of the different components [45]. In Fig. 2 the Raman images obtaining by mapping the M70PLA as well as the corresponding Raman spectra, are presented, evidencing the intensity of each signal. In particular, the green portion is related to the intensity of PCL signal from the band centered at 1109 cm-1. The red region is related to the intensity of PLA signal, centered in the band at 873 cm-1 [46]. In Fig. 3 the Raman images as well as the Raman spectra for the three different polymeric blends is reported. From this analysis it is clear that a phase-separated morphology clearly exists for the three different blends, and it is possible to detect both the PLA-reach phase and the PCL-rich phase. Moreover, it is worth to note that accordingly with the FE-SEM images, the three blends present a phase separation distribution completely different. In particular the dark regions of the Raman images (Fig. 3) correspond to the region in which both polymers exist, as can be confirmed also by Raman spectra in which both PLA and PCL centered bands has been obtained. For M70PLA can be appreciated that PLA forms a continuous phase (red regions of Fig. 3) with dispersed spheres of PCL with different sizes (green regions of Fig. 3). On the contrary, for M50PLA, two well differentiated areas of each homopolymer are detected, indicating the existence of large domains of each homopolymer. Finally, M30PLA presents the PCL continuous region with irregular PLA small domains of different sizes. Regarding to the dark regions of the figures, which correspond to points with the contribution of both PCL and PLA homopolymer, M70PLA presents the largest ones, suggesting a better compatibilization in the interphase between the two different homopolymers. Thus, RAMAN maps are well related with the morphology previously obtained from the FE-SEM images.

In Fig. 4a the TGA experiments for all the samples are shown. It can be noted that the PLA degradation occurs at lower temperatures, at around 350 °C (black line), while the PCL degradation (orange line) takes place at around 400 °C. For a better visualization of the degradation steps, in Fig. 4b the normalized derivative of the weight loss (DTG) curves of Fig. 4a are presented. The maximum degradation temperature of PLA in the blends (TPLA) is around 355 C while for PCL (TPCL) is 393°C. Moreover, regarding the DTG curves, the contribution to the degradation of both homopolymers in the blends can be observed, which allows determining the amount of each homopolymer in the blend. In Table 2 the results obtained from the DTG curves of Fig. 4b are summarized. The amounts of each polymer in the blend were calculated by fitting both curves to a Gaussian functions and studying the area below of each curve. It is worth to note that the real amount of each homopolymer is (third and fourth columns of Table 2) in good agreement with the theoretical ones (second column of Table 2), thus indicating that the feeding of the blend during the processing was accurate. The temperature corresponding to the degradation of 5% of the sample (T5%) for the blends, is higher than for the pristine PLA, indicating that the PCL addition improve the thermal stability of PLA.

Dynamic DSC measurements were performed to check the thermal properties and the melt/crystallization behavior of both PCL and PLA in the polymeric blends. In Fig. 5 the results for the thermal cycles (heating-cooling-heating) performed on all the materials are represented. The first heating, reported in Fig. 5a, shows the thermal properties of the blends as obtained after the processing. All the blends present the melting peak of PCL around 60 °C and the melting peak of PLA at about 150 °C. Moreover, the cold crystallization of PLA is also observed in the first heating scan, indicating that the PLA did not reach the fully degree of crystallinity during the cooling after the processing. It is worth to note that the Tg of the pristine PLA (M100PLA) appears around 60 °C making difficult to determine it during the heating scans for the blends due to its overlapping with the melting temperature of PCL. However, it is worth to note that M70PLA is the blend with the higher amount of crystalline PLA. This result is very important in order to study the shape memory behavior of the blends, where, the crystalline phase of PLA is the fixing phase, while the crystalline phase of PCL is the switching phase and the Tm of PCL is the transition temperature. In Fig. 5b the cooling scans of each blend are reported. It is worth to note that, under these experimental conditions (cooling at 10 °C/min), the PCL crystallizes completely while the PLA does not crystallize, neither in the blends nor in the neat material. This fact evidences the different crystallization behavior of PLA compared with the PCL. Moreover, the PCL crystallization of M70PLA presents a different trend compared to the other blends, showing two crystallization peaks. The presence of these two peaks could be related to the presence of two different kinds of crystals, but the presence of only one melting peak for the PCL in the second heating scan (Fig. 5c) is not compatible with this phenomenon. Thus, the formation of these two crystallization peaks can be related to the high content of PLA in the blend which difficult the reorganization of PCL chains for crystallizing. In Fig. 5c the second heating scans is represented, showing the thermal behavior of the materials after erasing their thermal history. The inset of Fig. 5c corresponds to the range of PCL Tg at around A63 C. The data shown in Table 3 were extracted from the second heating scan.

The Tg of PCL and the Tm values for both PCL and PLA homopolymers are not strongly affected by the blend compositions thus indicating their immiscibility [25,47]. The Tc of PCL remains partially constant for all the blend compositions while the cold crystallization temperature (Tcc) of PLA slightly decreases by decreasing the amount of PLA in the blend. This fact, as well as the slightly increase of the degree of crystallinity of PLA by increasing the PCL content, suggests that the presence of PCL favors the crystallization of PLA, acting as nucleate agent. Similar results have been evidenced for PLA blended with other polymers [48].

The dynamic mechanical behavior of the blends and the pristine homopolymers are shown in Fig. 6, where the curves are divided in two plots, corresponding to the storage modulus in the region of the Tg of PCL and PLA, Fig. 6a and b, respectively, while in Fig. 6c and tan d for the same temperature regions are reported. Regarding the storage modulus and tan d profile in the PCL regions, the glass transition temperature of PCL starts around -60 °C for all the blends, thus obtaining that the higher is the PCL content the stronger is the

peak. In the region of the Tg of PLA two phenomena can be appreciated, the relaxation of PLA due to the Tg as well as the melting of PCL. The melting of PCL can be noted by a big decrease in the storage modulus (Fig. 6b). This drop is higher for M30PLA. Regarding the tan d curves (Fig. 6d), the Tg of M100PLA starts at about 45°C and takes the maximum value at 60 °C. But, for the blends the values are increased of about 5 °C, indicating the presence of the melting of PCL and confirming that both processes are overlapped as it occurs for the DSC experiments. From 70 °C the storage modulus curves increased for all the blends and in particular for the neat PLA, indicating the beginning of the cold crystallization process of PLA.

The mechanical properties were determined by tensile tests and the stress-strain curves are shown in Fig. 7. Due to the high deformation of some blends the plot was split, making easier to visualize the behavior of the samples at low strains. As it is shown in Fig. 7, M100PLA reaches larger values of stress, while M0PLA reaches the largest value of maximum elongation at break. The three different blends show an intermediate behavior. In Table 4 are summarized the mechanical properties of the blends, in term of elastic modulus, tensile stress and elongation at break, extracted from the stress-strain curves of Fig. 7. The sample M50PLA presents an unexpected behavior as it does not show a clear necking formation and the maximum strain reached was the lowest one. This singular behavior suggests that at nano/microlevel some morphological changes occurred including macro segregation. This is well related to the results merged from the morphology analysis, which showed that at this concentration the blend presents a co-continuous morphology, with large regions of each homopolymer. Moreover, M50PLA shows the lowest value of elongation at break, comparing to the other blends, due to the phase separation and the poor adhesion between both homopolymers at this concentration. A similar behavior for PCL and PLA blends was reported by Chen et al. where a PLLA/PCL sample of 50 wt % of PLLA show lower elongation at break than the blend with 60 wt % of PLLA [12]. As expect, the elastic modulus, decreases when the PCL content increases, due to the plasticizer effect of the PCL, as reported also by Simoes et al. [23]. Once characterized the different materials, focusing the attention on the mechanical response and on the crystallinity behavior of the blends, the thermally-activated shape memory effect was studied. Only M70PLA shows shape memory properties (Fig. 8) at about 55 °C. The other ones were evaluated, but they broke during the first elongation step so, it was impossible to perform the shape memory analysis. This fact can be explained thus taking into account the first heating DSC scan, where M70PLA show the higher amount of crystalline phase, acting as the fixing phase. It is important to note that in order to study the shape memory behavior, the first DSC scan has to be taken into account, thus considering that no other thermal treatments have been performed on the blends. Both M30PLA and M50PLA are not able to fix the transient shape due to the low amount of crystalline PLA phase.

Moreover, in the case of M50PLA the mechanical properties strongly decreased, hindering the shape fixation without break the sample. Therefore, only M70PLA presents shape memory behavior. The digital photographs of Fig. 8 correspond to M70PLA. It was heated at 55 °C and deformed and then cooled down,

reaching the deformed shape reported on the left. Heating again at 55 °C, the crystalline PCL melts and the sample recovers their initial shape as it is clearly shown in the photograph sequences of Fig. 8. Shape memory test was designed for quantifying the shape memory capability of M70PLA. The thermo-mechanical cycles of the experiment was performed at 55 C, closed to the melting temperature of PCL. During the test, the specimen, clamped into the tensile tester, was heated at a 55 C for 10 min. Then, the specimen was stretched until 50% (εm) by applying a constant deformation stress. Once the εm was reached, after two minutes at 55 °C, the sample was cooled down to about 15 C for further 6 min under the same constant stress and after that the stress was released. At this point the temporary shape has been fixed (εu). Finally, upon heating the sample at 55 C for 10 min the initial shape was recovered, characterized by the elongation reached at the end of the cycle (εp).

Afterwards, another thermo-mechanical cycle was started. The shape memory cycles are shown in Fig. 9. The two cycles reported in the figure demonstrate the ability of the blend M70PLA to fix the temporary shape and to recover its initial shape. However, during the second thermo-mechanical cycle the stress reached is lower compared with the stress obtained during the first one. Finally, in the third cycle the sample broke. The values of the shape recovery ratio (Rr) and the shape fixity ratio (Rf) for the two cycles are summarized in Table 5, confirming the excellent ability to fix the temporary shape, with Rf higher than 96%. Also the ability to recover the initial shape is quite good. Rr in fact, is very high during the first cycle, more than 80%, and decreases at 77% after the second thermo-mechanical cycle. One of the most important application fields for PCL, PLA and their blends is biomedicine [3] as well as food packaging [48]. For this reason, a degradation study of these materials was performed in this article. In particular, the hydrolytic degradation was performed using a phosphate buffer solution (pH ¼ 7.2e7.4) at 37 °C. In Fig. 10a, the values of the weight loss of the samples after each incubation time are reported. M100PLA, and M70PLA did not lose weight after 20 weeks of experiment (stars and down triangles, respectively). On the contrary, M0PLA, M30PLA and M50PLA lose a 3 wt % after 20 weeks (squares, dots and up triangles) of experiment.

The GPC analysis allows checking the variations on the molecular weight (Mn) produced after the degradation process, considering that the low Mn species appear at higher elution times. In Fig. 10b the GPC profiles of M0PLA, M50PLA and M100PLA after each month of degradation are reported. As it is shown in the figure, the Mn of PLA (M100PLA) is slightly decreased after few months and the highest variation was found at the fourth month. For M50PLA the reduction is lower and for M0PLA is almost impossible to clearly distinguish any variations during the 5 months analyzed. The calculated values from GPC experiments are summarized in Table 6.

From the weight loss values for the samples and the GPC data it emerges that PCL degrades by scission of end groups of the polymer chain, which can be dissolved in water and disappeared when the samples were washed and dried after the experiment. Similar results were presented for Lam et al. for PCL scaffolds

during an in vitro and in vivo tests, where a variation of weight loss around 2.6% is presented without variations in the molecular weight [49]. For this reason the molecular weight of M0PLA does not change considerably even if the weight of the samples decreases a 3 wt %. On the contrary, the degradation mechanism of PLA is completely different and it seems that PLA degrades by chain scission of the polymer chains, but these chains remained and did not disappear during the washing of the sample. This fact explains the decrease on Mn without weight loss. Finally M50PLA shows an intermediate behavior, concluding that in the blends each homopolymer degrade following the same mechanism of the pristine homopolymers. The degradation test performed under composting conditions at lab-scale was obtained by following the procedure of the EN ISO 20200. The experiments were performed during 4 week thus analyzing one sample after each incubation week. Five samples were prepared for each week (week 0, week 1, week 2, week 3, and week 4). In Fig. 11 the digital photographs for the degraded blends are shown. As it can be observed, M100PLA is transparent at week 0 but after one week become opaque and more fragile, indicating that PLA crystallized during this week, thus confirming the well-known phenomenon called chemo-crystallization, which is involved under these conditions [50]. Moreover, M100PLA is broken after 1 week, thus indicating the sample fragility achieved as consequence of the chain scission provoked during the degradation process. After four weeks no rest of the material were found indicating that the M100PLA is completely degraded. Regarding the compostability of the blends, it is easy to note that all of them present evident signs of degradation thus starting from the second week, such as sample fractures and superficial changes as well as thinner samples. It is clear that the addition of PCL prevents the composting degradation of PLA, delaying the degradation. The degradation of PLA in composting conditions was evaluated by GPC measurements, Fig. 12a for M100PLA and Fig. 12b for M50PLA. The increase in the elution time reflects the reduction of the molecular weight due to the hydrolysis of the polymer chains under composting conditions. For M100PLA, itsMn is reduced, after each week. In particular, during the second week, the presence of three different peaks can be noted, thus confirming the wide polydispersity of the PLA polymer chains provoke by the degradation process. At least, in the third week the lowest molecular weight for the PLA is reached. From M50PLA, Fig. 12b, it is possible to note that both homopolymers degrade with different rate. In particular, the peaks and the shoulders at higher elution times correspond to the PLA degraded polymer chains, while the peaks at smaller elution times correspond to the molecular weight distribution of PCL. Therefore, it is possible to observe that PCL degrade slower than PLA, thus considering that the PCL peaks shift to higher elution times, but very slowly. The last technique used to visualize the composting degradation was the FT-IR. Finally, by infrared spectra, M100PLA (Fig. 13a and b) and M50PLA (Fig. 13c and d) have been also studied. The PLA spectra show clearly the degradation of the polymer chains. In Fig. 13a the wide signal centered at about 3300 cmA1 of the third week corresponds to the hydroxyl groups due to the hydrolysis of the PLA chains. Moreover, the

signal of about 1043 cm-1, Fig. 13b, appears broader in the samples with more weeks in composting degradation, thus indicating that the polymer chains are shorter.

From the M50PLA spectra presented in Fig. 13c it is possible to confirm that the degradation process occurs slowly due to the addition of PCL, as it was previously obtained by GPC analysis. In fact, it is worth to note that the carbonyl band of PLA, which appears at about 1750 cm-1, decreases faster compared with the PCL band at 1725 cm-1, indicating that the PLA degrades quickly. In addition, in Fig. 13d the band of PLA at 1087 cmA1 strongly decreases after only one week of composting conditions. However, the presence of PCL reduces the degradation of PLA, in agreement with the results previously obtained from the GPC analysis.

4. Conclusions

In this work, biodegradable PLA/PCL blends were processed and they were fully characterized. The morphology studies were carried out by FE-SEM, and RAMAN spectroscopy, demonstrating that the blends are immiscible and showing a different phase separation depending on the amount of PCL in the blends. The thermal degradation of PLA was improved by the PCL addition, while the DSC measurements confirmed their immiscibility. The mechanical behavior demonstrated the possibility to design PCL/PLA blends with a wide range of mechanical properties depending on the blend composition. Shape memory of the processed blends was investigated finding that only the blend with 30 wt % of PCL show shape memory behavior. This particular effect was quantified by performing thermo-mechanical cycles, finding that the shape memory parameters are very good during two thermo-mechanical cycles. Due to degradability features of the homopolymers, two degradation tests were carried out, under composting conditions as well as in vitro. The materials degrade under composting conditions with different rate as demonstrated by the GPC measurements. In particular, the PCL addition prevents the degradation of PLA under composting conditions. On the other hand, the in vitro degradation tests show that under these conditions the materials degrade slower than in the degradation under composting conditions. Actually, the data suggests that PCL degrades by chain scission of the end groups, with a slightly weight lost and maintaining quite constant the molecular weight while PLA degrades by chain scission of polymer chains with a decrease of molecular weight but without weight loss. The results reported here indicate the possibility to design biodegradable multifunctional blends by a low cost and an easy scalable process. These blends, which show a wide range of mechanical behavior, degradation rates and even shape memory ability, can cover a wide range of applications, from biomedical to packaging applications.

Acknowledgments

We are indebted to the Spanish Ministry of Economy and Competitiveness, MINECO (MAT2013-48059-C2-1-R and MAT2014-55778-REDT) and to the Regional Government of Madrid (S2013/ MIT-2862) for their economic support. L.P. acknowledges MINECO for the “Ramon y Cajal” contract (RYC-2014-15595).

References

[1] J.M. Raquez, R. Narayan, P. Dubois, Recent advances in reactive extrusion processing of biodegradable polymer-based compositions, Macromol. Mater. Eng. 293 (2008) 447-470.

[2] X. Tang, S. Alavi, Recent advances in starch, polyvinyl alcohol based polymer blends, nanocomposites and their biodegradability, Carbohydr. Polym. 85 (2011) 7e-16.

[3] B.D. Ulery, L.S. Nair, C.T. Laurencin, Biomedical applications of biodegradable polymers, J. Polym. Sci. Part B Polym. Phys. 49 (2011) 832-864.

[4] I. Vroman, L. Tighzert, Biodegradable polymers, Materials 2 (2009) 307-344.

[5] P. Lovell, in: M.J. Folkes, P.S. Hope (Eds.), Polymer Blends and Alloys, Chapman and Hall, London, 1993.

[6] M.P. Arrieta, J. L opez, D. L opez, J.M. Kenny, L. Peponi, Development of flexible materials based on plasticized electrospun PLA-PHB blends: structural, thermal, mechanical and disintegration properties, Eur. Polym. J. 73 (2015) 433-446.

[7] M.P. Arrieta, M.D.M. Castro-Lopez, E. Ray on, L.F. Barral-Losada, J.M. L opez- Vilarino, J. Lopez, et al., Plasticized poly(lactic acid)-poly(hydroxybutyrate) (PLA-PHB) blends incorporated with catechin intended for active foodpackaging applications, J. Agric. Food Chem. 62 (2014) 10170-10180.

[8] L. Peponi, D. Puglia, L. Torre, L. Valentini, J.M. Kenny, Processing of nanostructured polymers and advanced polymeric based nanocomposites, Mater. Sci. Eng. R Rep. 85 (2014) 1-46.

[9] D. Wu, Y. Zhang, M. Zhang, W. Zhou, Phase behavior and its viscoelastic response of polylactide/poly (ε-caprolactone) blend, Eur. Polym. J. 44 (2008) 2171-2183.

[10] L. Zhang, S. Goh, S. Lee, Miscibility and crystallization behaviour of poly (Llactide)/ poly (p-vinylphenol) blends, Polymer 39 (1998) 4841-4847.

[11] O. Persenaire, J.M. Raquez, L. Bonnaud, P. Dubois, Tailoring of co-continuous polymer blend morphology: joint action of nanoclays and compatibilizers, Macromol. Chem. Phys. 211 (2010) 1433-1440.

[12] C.-C. Chen, J.-Y. Chueh, H.-M. Huang, S.-Y. Lee, Preparation and characterization of biodegradable PLA polymeric blends, Biomaterials 24 (2003) 1167-1173.

[13] F. Cock, A. Cuadri, M. García-Morales, P. Partal, Thermal, rheological and microstructural characterisation of commercial biodegradable polyesters, Polym. Test. 32 (2013) 716-723.

[14] C. Elds€ater, B. Erlandsson, R. Renstad, A.-C. Albertsson, S. Karlsson, The biodegradation of amorphous and crystalline regions in film-blown poly (ε-caprolactone), Polymer 41 (2000) 1297-1304.

[15] G. Maglio, A. Migliozzi, R. Palumbo, B. Immirzi, M.G. Volpe, Compatibilized poly (ε-caprolactone)/poly (l-lactide) blends for biomedical uses, Macromol. Rapid Commun. 20 (1999) 236-238.

[16] M. Vert, S. Li, G. Spenlehauer, P. Gu erin, Bioresorbability and biocompatibility of aliphatic polyesters, J. Mater. Sci. Mater. Med. 3 (1992) 432-446.

[17] A.C. Albertsson, R. Renstad, B. Erlandsson, C. Elds€ater, S. Karlsson, Effect of processing additives on (bio) degradability of film-blown poly (ε-caprolactone), J. Appl. Polym. Sci. 70 (1998) 61-74.

[18] K. Fukushima, C. Abbate, D. Tabuani, M. Gennari, P. Rizzarelli, G. Camino, Biodegradation trend of poly (ε-caprolactone) and nanocomposites, Mater. Sci. Eng. C 30 (2010) 566-574.

[19] I. Moura, A. Machado, F. Duarte, R. Nogueira, Biodegradability assessment of aliphatic polyesters-based blends using standard methods, J. Appl. Polym. Sci. 119 (2011) 3338-3346.

[20] J.M. Raquez, Y. Habibi, M. Murariu, P. Dubois, Polylactide (PLA)-based nanocomposites, Prog. Polym. Sci. 38 (2013) 1504-1542.

[21] R. Renstad, S. Karlsson, Å. Sandgren, A.-C. Albertsson, Influence of processing additives on the degradation of melt-pressed films of poly (ε-caprolactone) and poly (lactic acid), J. Environ. Polym. Degrad. 6 (1998) 209-221.

[22] P. Sarazin, G. Li, W.J. Orts, B.D. Favis, Binary and ternary blends of polylactide, polycaprolactone and thermoplastic starch, Polymer 49 (2008) 599-609.

[23] C. Simoes, J. Viana, A. Cunha, Mechanical properties of poly (ε-caprolactone) and poly (lactic acid) blends, J. Appl. Polym. Sci. 112 (2009) 345-352.

[24] N. L opez-Rodríguez, A. L opez-Arraiza, E. Meaurio, J. Sarasua, Crystallization, morphology, and mechanical behavior of polylactide/poly (ε-caprolactone) blends, Polym. Eng. Sci. 46 (2006) 1299-1308.

[25] Y. Zhang, D. Wu, M. Zhang, W. Zhou, C. Xu, Effect of steady shear on the morphology of biodegradable poly (ε-caprolactone)/polylactide blend, Polym. Eng. Sci. 49 (2009) 2293-2300.

[26] R. Salehiyan, K. Hyun, Effect of organoclay on non-linear rheological properties of poly (lactic acid)/poly (caprolactone) blends, Korean J. Chem. Eng. 30 (2013) 1013-1022.

[27] J.M. Raquez, S. Vanderstappen, F. Meyer, P. Verge, M. Alexandre, J.M. Thomassin, et al., Design of cross-linked semicrystalline poly(ε-caprolactone)- based networks with one-way and two-way shape-memory properties through Diels-Alder reactions, Chem. A Eur. J. 17 (2011) 10135-10143.

[28] M.D. Hager, S. Bode, C. Weber, U.S. Schubert, Shape memory polymers: past, present and future developments, Prog. Polym. Sci. 49e50 (2015) 3-33.

[29] I. Navarro-Baena, J.M. Kenny, L. Peponi, Thermally-activated shape memorybehaviour of bionanocomposites reinforced with cellulose nanocrystals, Cellulose 21 (2014) 4231-4246.

[30] L. Peponi, I. Navarro-Baena, J.M. Kenny, Shape memory polymers: properties, synthesis and applications, Smart Polym. Appl. (2014) 204-236.

[31] C. Samuel, S. Barrau, J.M. Lefebvre, J.M. Raquez, P. Dubois, Designing multipleshape memory polymers with miscible polymer blends: evidence and origins of a triple-shape memory effect for miscible PLLA/PMMA blends, Macromolecules 47 (2014) 6791-6803.

[32] L. Peponi, I. Navarro-Baena, A. Sonseca, E. Gimenez, A. Marcos-Fernandez, J.M. Kenny, Synthesis and characterization of PCLePLLA polyurethane with shape memory behavior, Eur. Polym. J. 49 (2013) 893-903.

[33] N.I. Akos, M.U. Wahit, R. Mohamed, A.A. Yussuf, Preparation, characterization, and mechanical properties of poly (ε-caprolactone)/polylactic acid blend composites, Polym. Compos. 34 (2013) 763-768.

[34] H.-T. Liao, C.-S. Wu, Preparation and characterization of ternary blends composed of polylactide, poly (3-caprolactone) and starch, Mater. Sci. Eng. A 515 (2009) 207-214.

[35] Y.-H. Na, Y. He, X. Shuai, Y. Kikkawa, Y. Doi, Y. Inoue, Compatibilization effect of poly (ε-caprolactone)-b-poly (ethylene glycol) block copolymers and phase morphology analysis in immiscible poly (lactide)/poly (ε-caprolactone) blends, Biomacromolecules 3 (2002) 1179-1186.

[36] V.B. Carmona, A.C. Corr^ea, J.M. Marconcini, L.H.C. Mattoso, Properties of a Biodegradable Ternary Blend of Thermoplastic Starch (TPS), Poly (ε-Caprolactone)(PCL) and Poly (Lactic Acid)(PLA), J. Polym. Environ. 23 (2015) 83-89.

[37] S. Han, T.J. Moon, Y.C. Bae, S. Yi, S.H. Lee, Composition dependence of rheological properties of polymer blends, Polymer 39 (1998) 1113-1117.

[38] L. Gardella, M. Calabrese, O. Monticelli, PLA maleation: an easy and effective method to modify the properties of PLA/PCL immiscible blends, Colloid Polym. Sci. 292 (2014) 2391-2398.

[39] L. Peponi, A. Tercjak, L. Torre, J.M. Kenny, I. Mondragon, Morphological analysis of self-assembled SIS block copolymer matrices containing silver nanoparticles, Compos. Sci. Technol. 68 (2008) 1631-1636.

[40] L. Peponi, A. Tercjak, R. Verdejo, M.A. Lopez-Manchado, I. Mondragon, J.M. Kenny, Confinement of functionalized graphene sheets by triblock copolymers, J. Phys. Chem. C 113 (2009) 17973-17978.

[41] L. Peponi, L. Valentini, L. Torre, I. Mondragon, J.M. Kenny, Surfactant assisted selective confinement of carbon nanotubes functionalized with octadecylamine in a poly(styrene-b-isoprene-b-styrene) block copolymer matrix, Carbon 47 (2009) 2474-2480.

[42] J. Odent, Y. Habibi, J.M. Raquez, P. Dubois, Ultra-tough polylactide-based materials synergistically designed in the presence of rubbery ε-caprolactone- based copolyester and silica nanoparticles, Compos. Sci. Technol. 84 (2013) 86-91.

[43] O. Monticelli, M. Calabrese, L. Gardella, A. Fina, E. Gioffredi, Silsesquioxanes: novel compatibilizing agents for tuning the microstructure and properties of PLA/PCL immiscible blends, Eur. Polym. J. 58 (2014) 69-78.

[44] L. Peponi, I. Navarro-Baena, J.E. B aez, J.M. Kenny, A. Marcos-Fern andez, Effect of the molecular weight on the crystallinity of PCL-b-PLLA di-block copolymers, Polymer 53 (2012) 4561-4568.

[45] S. Huan, W. Lin, H. Sato, H. Yang, J. Jiang, Y. Ozaki, et al., Direct characterization of phase behavior and compatibility in PET/HDPE polymer blends by confocal Raman mapping, J. Raman Spectrosc. 38 (2007) 260-270.

[46] G. Kister, G. Cassanas, M. Bergounhon, D. Hoarau, M. Vert, Structural characterization and hydrolytic degradation of solid copolymers of d, l-lactide-co- ε-caprolactone by Raman spectroscopy, Polymer 41 (2000) 925-932.

[47] J.-T. Yeh, C.-J. Wu, C.-H. Tsou, W.-L. Chai, J.-D. Chow, C.-Y. Huang, et al., Study on the crystallization, miscibility, morphology, properties of poly (lactic acid)/ poly (ε-caprolactone) blends, Polymer Plastics Technol. Eng. 48 (2009) 571-578.

[48] M.P. Arrieta, E. Fortunati, F. Dominici, E. Ray on, J. L opez, J.M. Kenny, Multifunctional PLA-PHB/cellulose nanocrystal films: processing, structural and thermal properties, Carbohydr. Polym. 107 (2014) 16-24.

[49] C.X. Lam, D.W. Hutmacher, J.T. Schantz, M.A. Woodruff, S.H. Teoh, Evaluation of polycaprolactone scaffold degradation for 6 months in vitro and in vivo, J. Biomed. Mater. Res. Part A 90 (2009) 906-919.

[50] M. Deroin e, A. Le Duigou, Y.-M. Corre, P.-Y. Le Gac, P. Davies, G. C esar, et al., Accelerated ageing of polylactide in aqueous environments: comparative study between distilled water and seawater, Polym. Degrad. Stab. 108 (2014) 319-329.

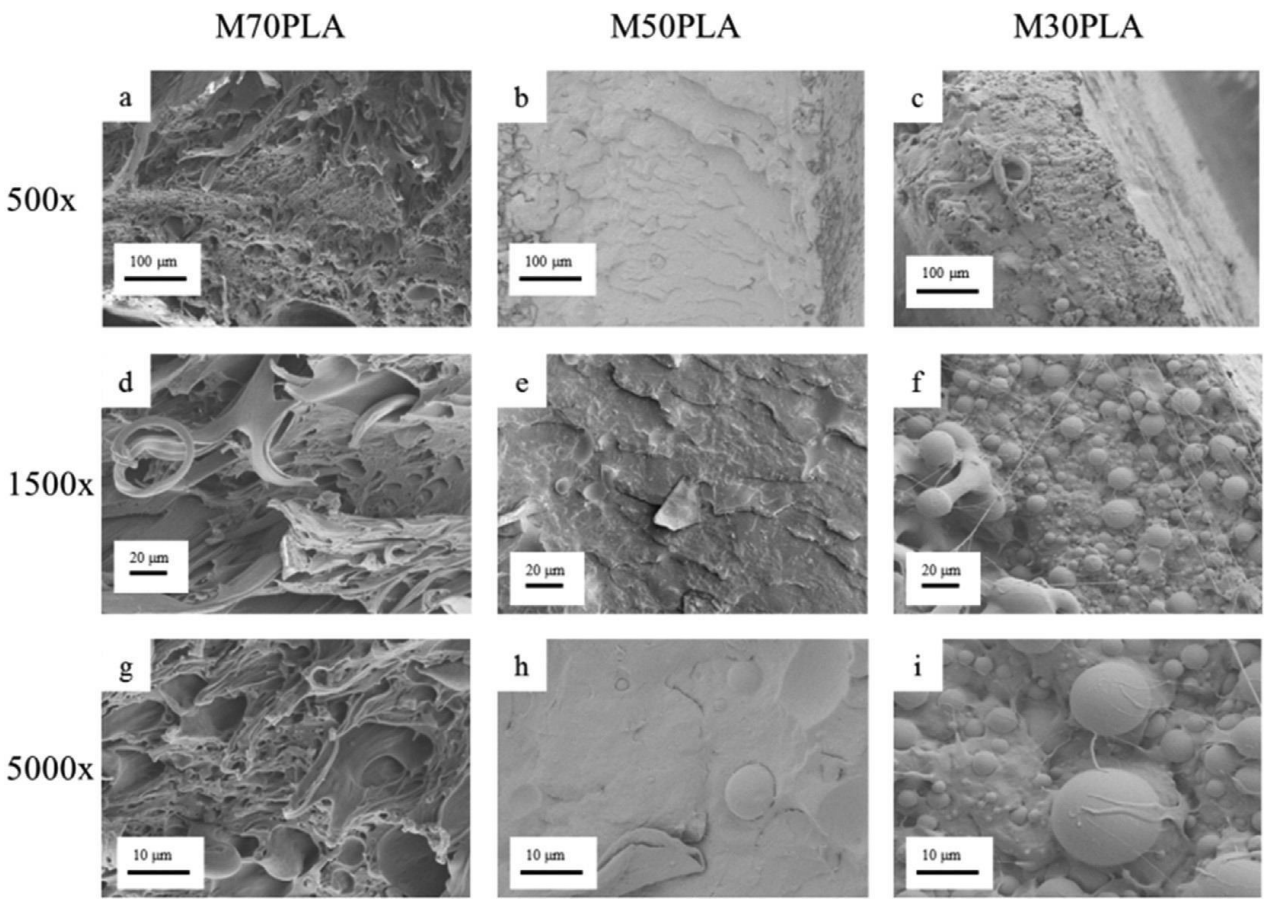

Fig. 1. SEM images of PLA/PCL blends at different magnifications: 500x (a, b and c), 1500x (d, e and f) and 5000x (g, h and i).

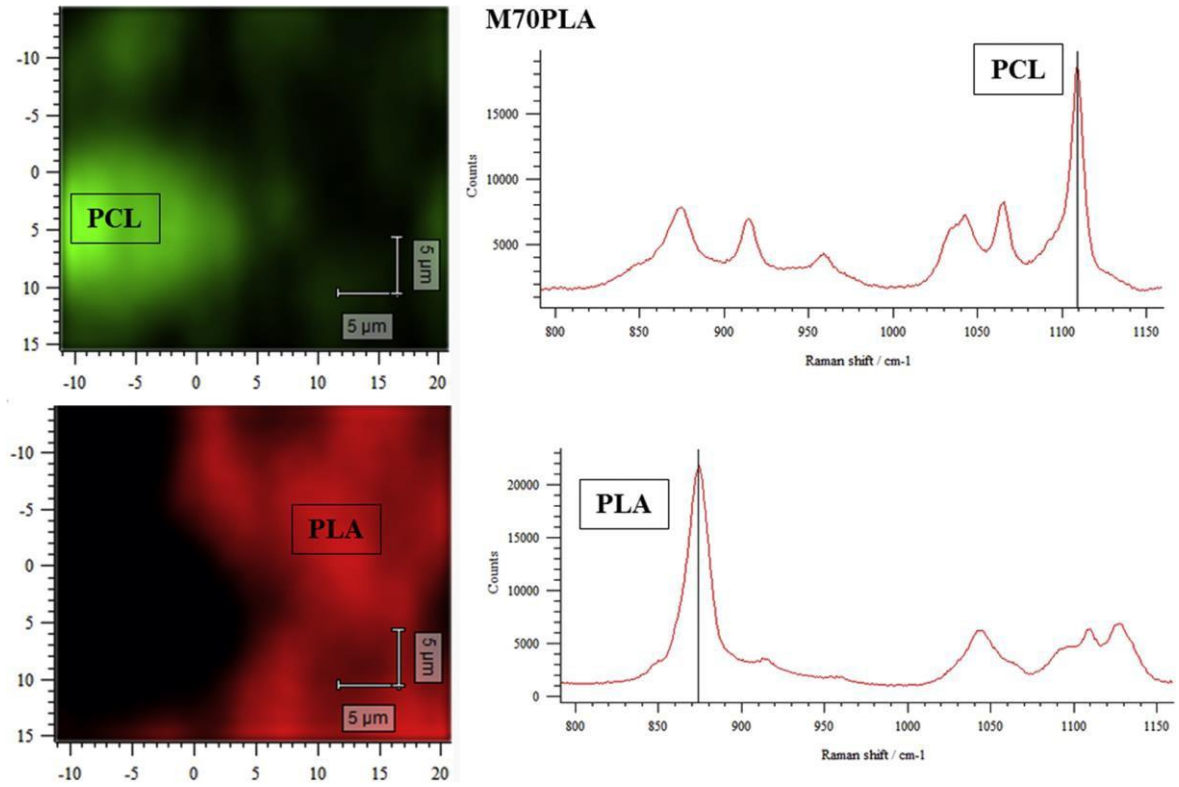

Fig. 2. On the top, Raman image at band 1109 cm^{-1} where the green portion is related to the intensity of PCL, with the corresponding Raman spectrum; at the bottom, Raman image at band 873 cm^{-1} where the red portion is related to the intensity of PLA with the corresponding Raman spectrum for the M70PLA. (For interpretation of the references to colour in this figure legend, the reader is referred to the web version of this article.)

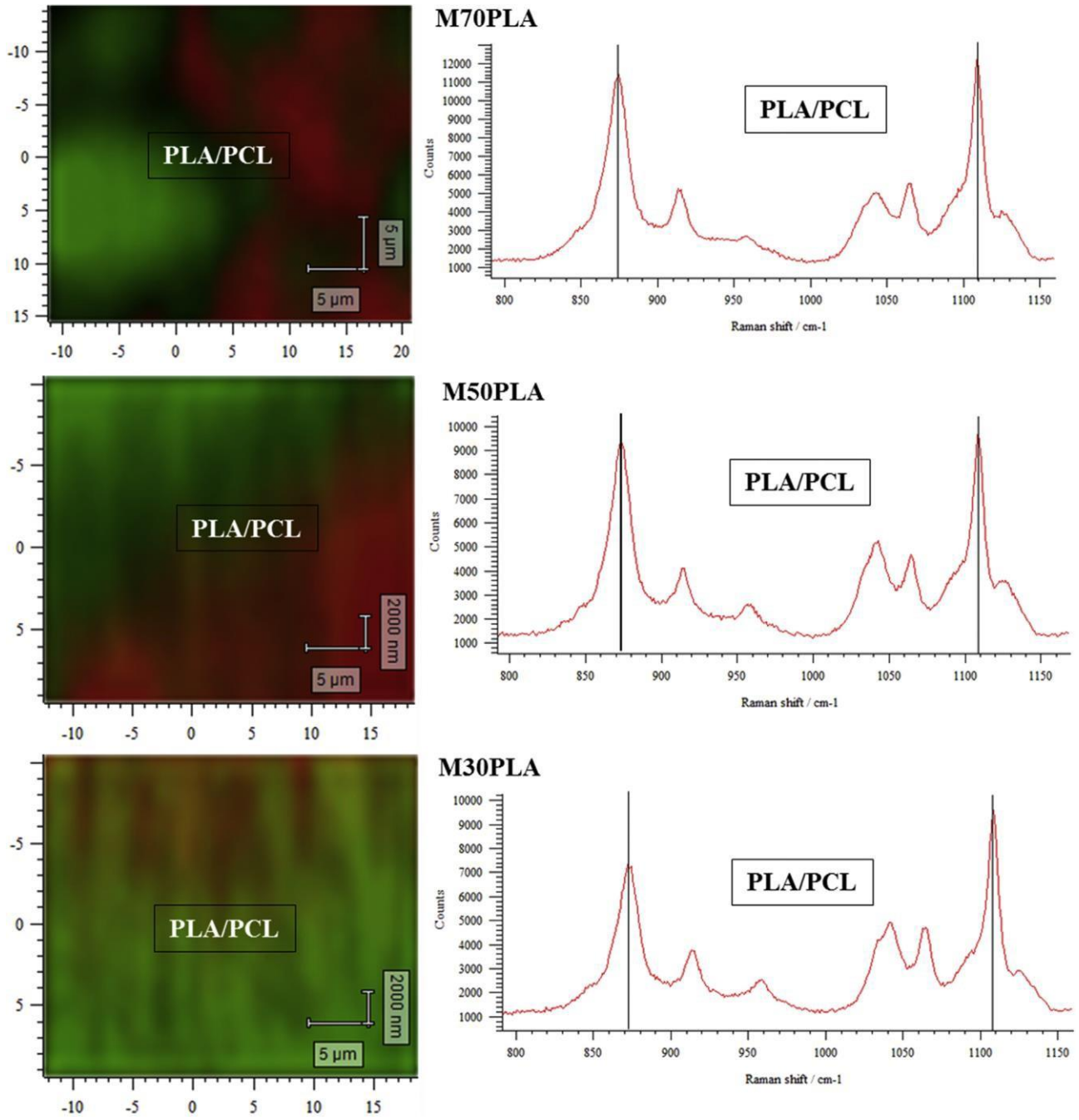

Fig. 3. Raman images with the corresponding Raman spectra for the three different blends.

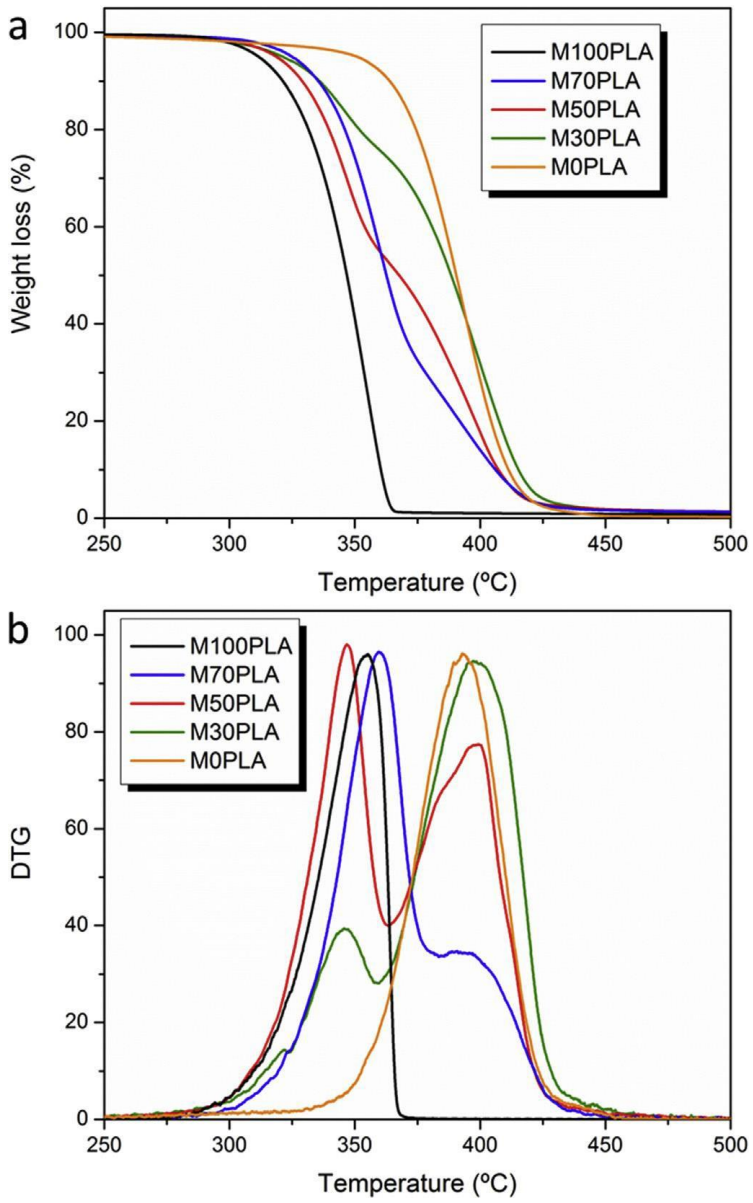

Fig. 4. Thermogravimetric analysis of the processed materials: a) weight loss profiles; b) normalized derivative of weight loss.

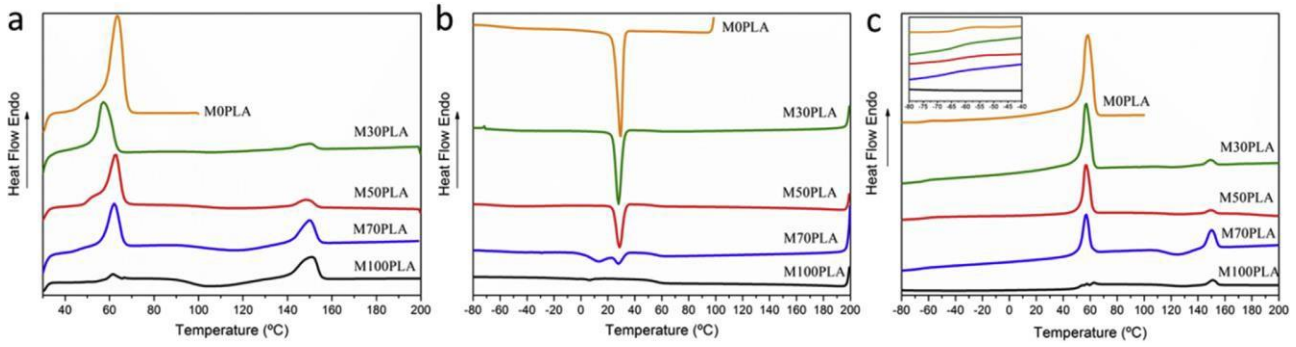

Fig. 5. DSC scans of processed materials: a) first heating scans; b) cooling scans; c) second heating scans. The inset of Fig. 5c corresponds to the Tg region of PCL

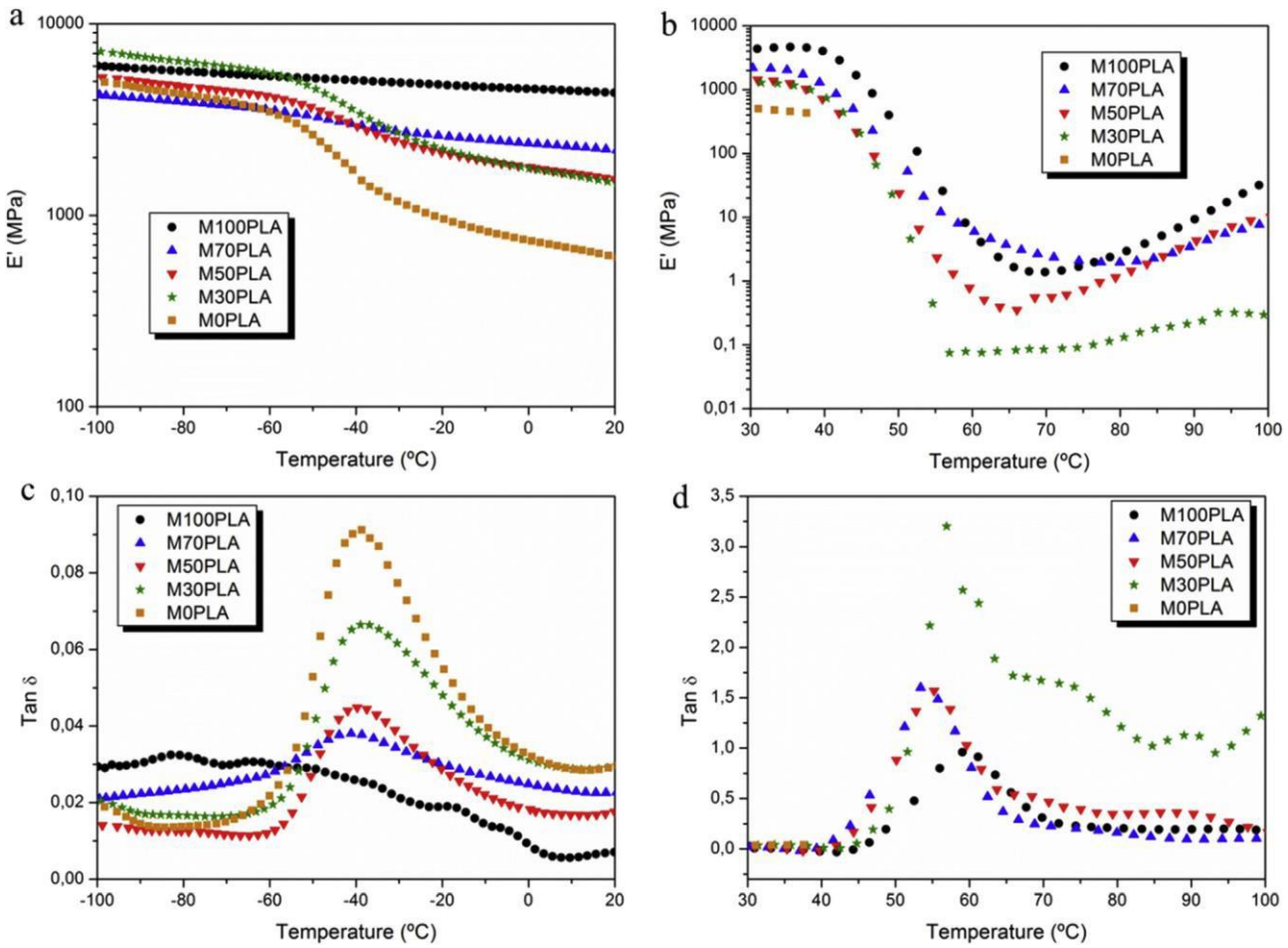

Fig. 6. Dynamical mechanical experiments in term of E0: a) region from-100 °C to 20 °C; b) region from 30 °C to 100 ° for E0; and Tan d: c) region from -100 °C to 20 °C; d) region from 30 °C to 100 °C.

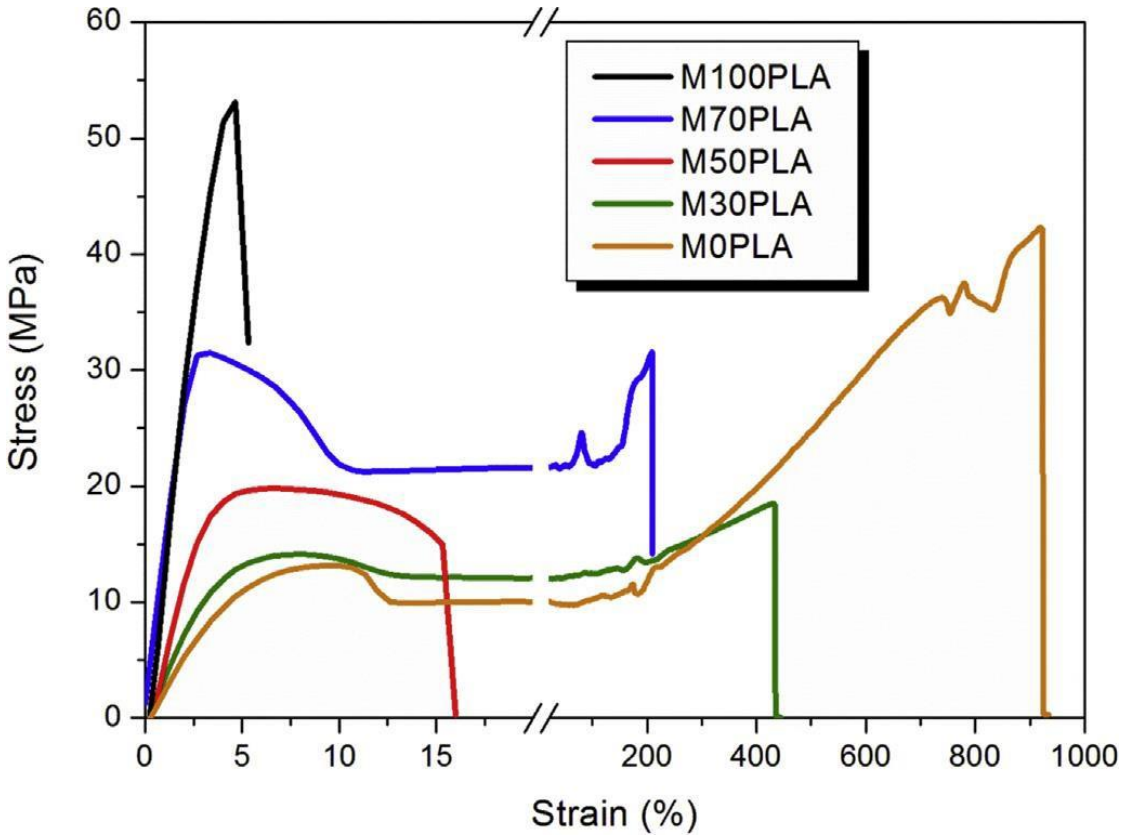

Fig. 7. Stress-Strain curves of the different materials.

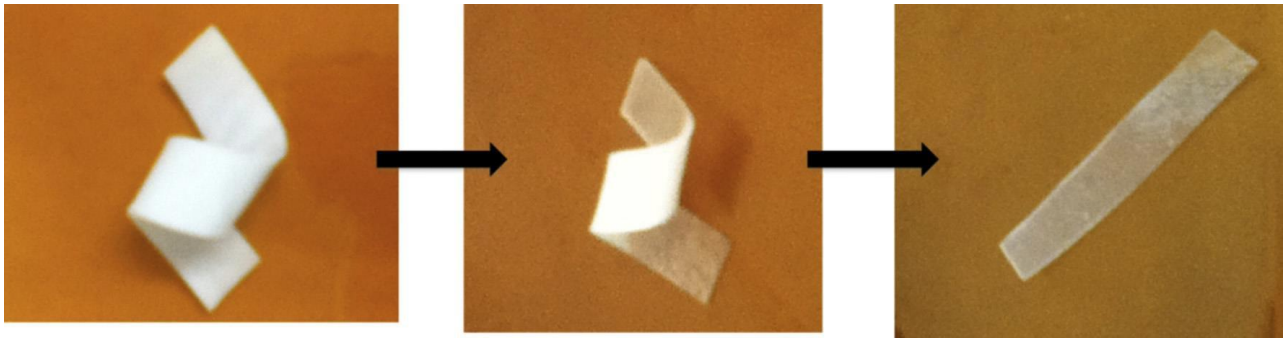

Fig. 8. Shape memory of M70PLA. The images show the recovery of the initial shape from the temporary state by heating application

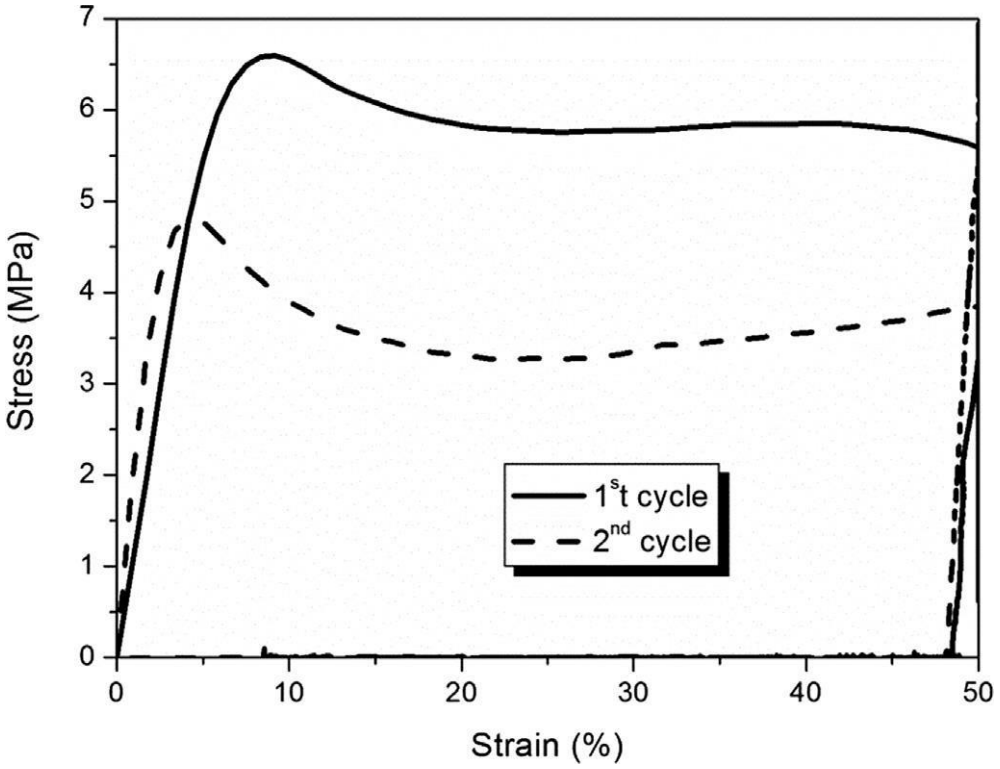

Fig. 9. Thermo-mechanical cycles for M70PLA at 55 °C.

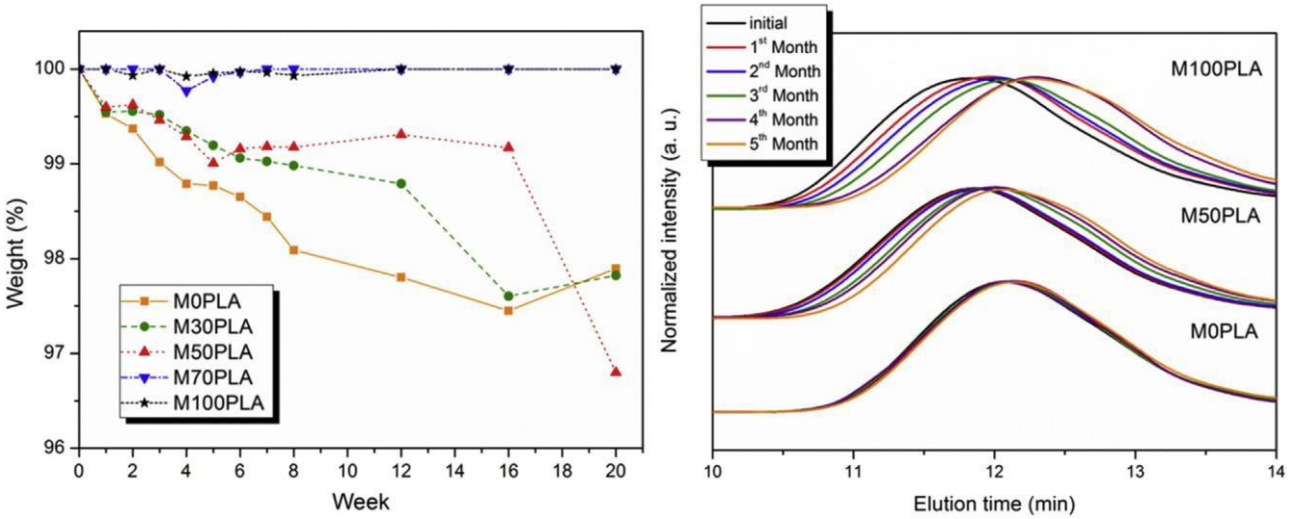

Fig. 10. Hydrolytic degradation: a)Weight loss after hydrolytic degradation at different incubation times for all the processed materials; b) GPC profiles for the different materials at each month.

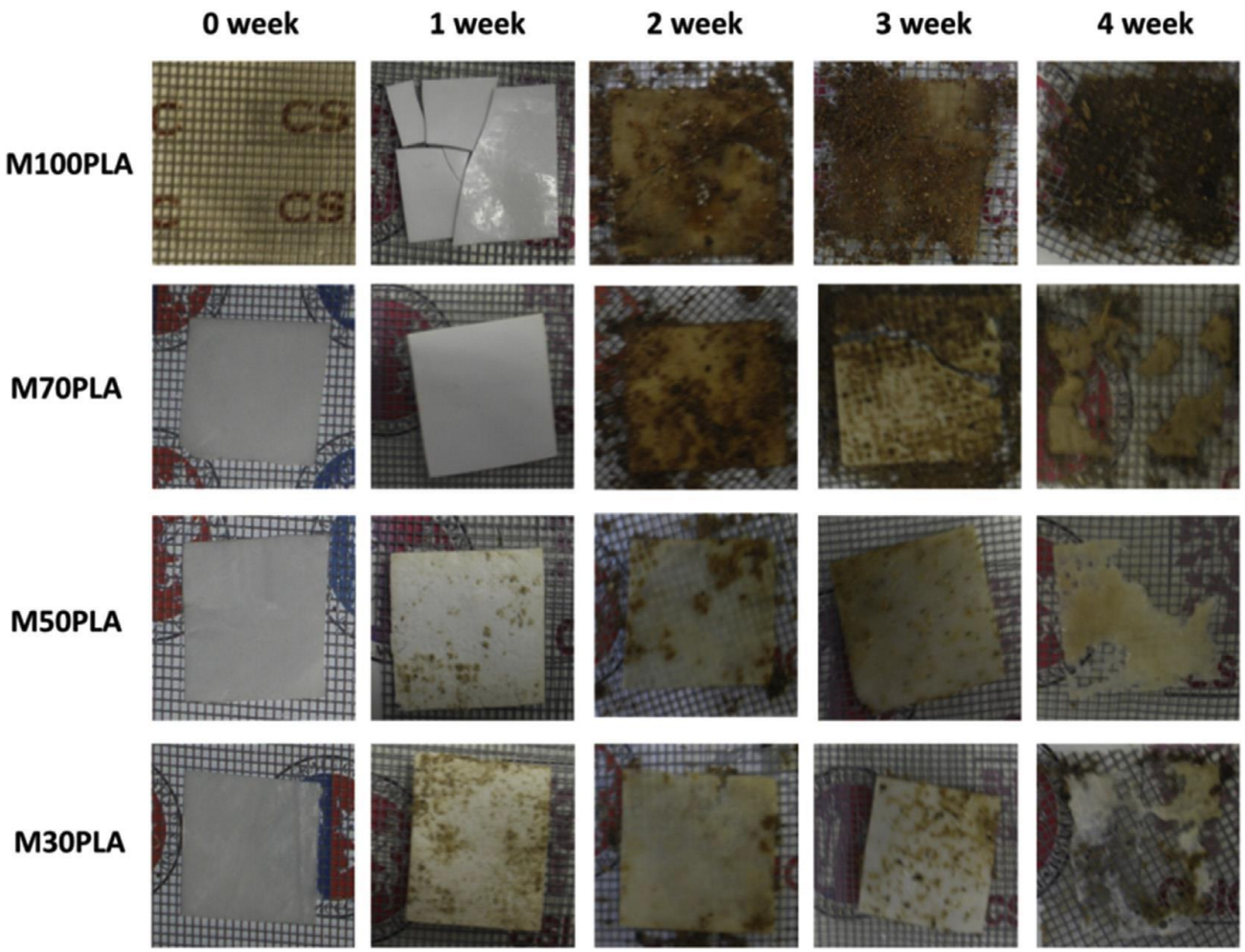

Fig. 11. Digital photographs of the samples corresponding to the processed materials after different incubation times

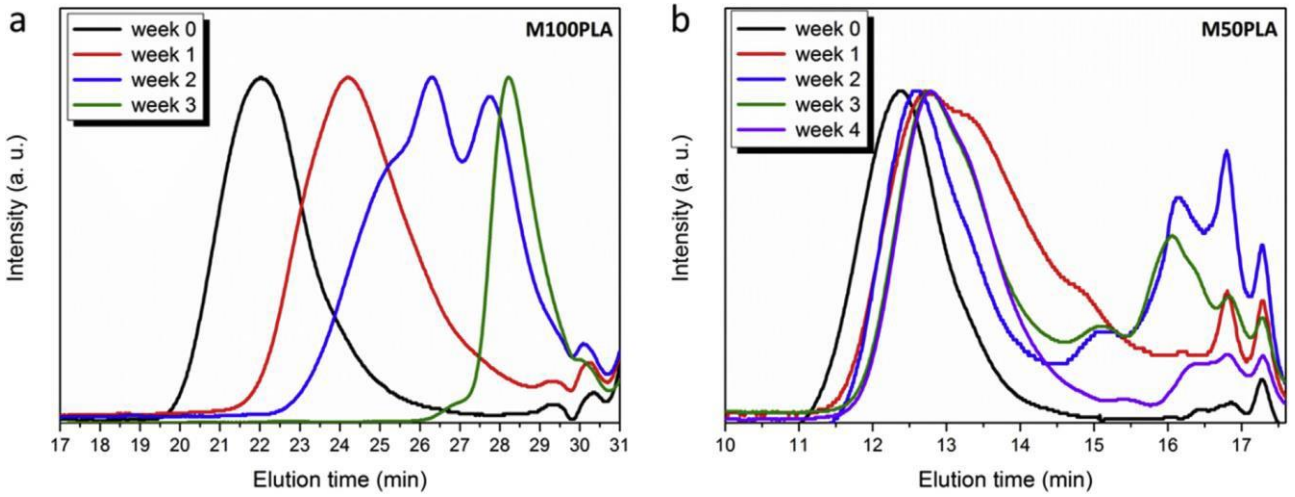

Fig. 12. GPC profiles for the composting degraded samples after different incubation times: a) M100PLA; b) M50PLA.

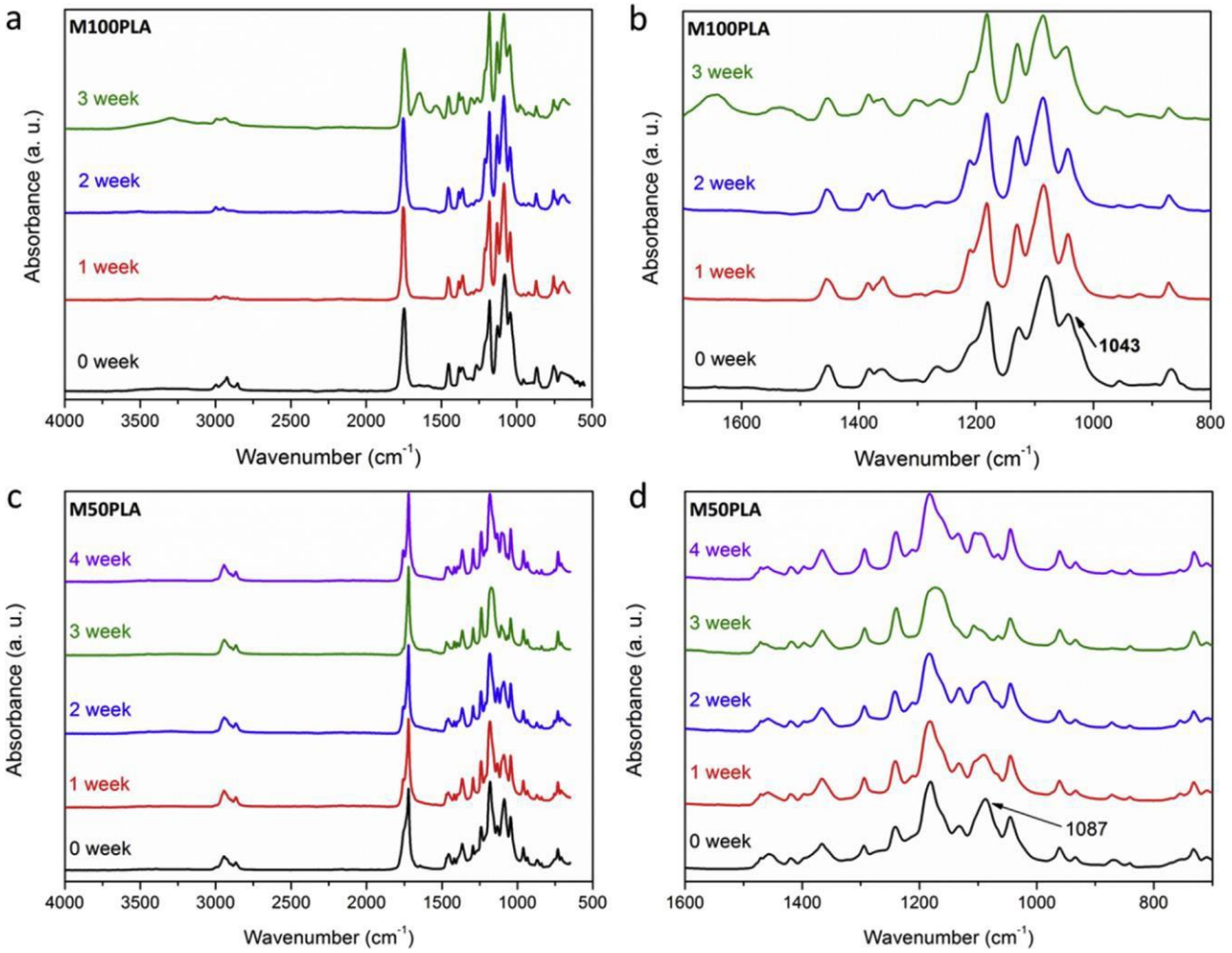

Fig. 13. Infrared measurements for the composting degraded samples at different incubation times: a) and b) M100PLA; c) and d) M50PLA.

Table 1: Compost composition according to ISO 20200.

Components	wt %
Sawdust	20
Rabbit food	15
Starch	5
Compost inoculum	5
Sugar	2.5
Oil	1.5
Urea	1
Water	50

Table 2: Thermogravimetric analysis results.

Sample	PCL/PLA	%PCL	%PLA	$T_{5\%}$ (°C)	T_{PCL} (°C)	T_{PLA} (°C)
M100PLA	0/100	0	100	312	–	355
M70PLA	30/70	29.7	70.3	321	395	359
M50PLA	50/50	48.8	51.2	319	399	345
M30PLA	70/30	69.6	30.4	325	398	345
M0PLA	100/0	100	0	355	393	–

Table 3: DSC results corresponding to the second heating scan.

Sample	PCL				PLA		
	T_m (°C)	T_c (°C)	X_c (%)	T_g (°C)	T_m (°C)	T_{cc} (°C)	X_c (%)
M100PLA	–	–	–	–	151	129	0.0
M70PLA	57	28	34	−66	150	125	0.5
M50PLA	57	29	34	−63	150	124	2.0
M30PLA	57	28	37	−66	150	122	3.4
M0PLA	58	29	41	−63	–	–	–

Table 4: Mechanical properties of PCL/PLA blends

Sample	Elastic modulus (MPa)	Max stress (MPa)	Elongation at break (%)
M100PLA	1670 ± 120	53 ± 3	5.3 ± 0.5
M70PLA	1241 ± 29	31 ± 2	199 ± 22
M50PLA	758 ± 51	21 ± 1	10 ± 4
M30PLA	400 ± 41	19 ± 2	422 ± 35
M0PLA	294 ± 18	41 ± 4	952 ± 23

Table 5: Values for Rr and Rf calculated from the thermo-mechanical cycles at 50% of deformation.

Cycle	R_r (%)	R_f (%)
1	83	97
2	77	96

Table 6: Molecular weight (Mn) and polydispersity index (PDI) for the different materials at each month.

Week	M0PLA		M50PLA		M100PLA	
	M_n (g/mol)	PDI	M_n (g/mol)	PDI	M_n (g/mol)	PDI
0	83,790	1.49	81,050	1.55	90,840	1.58
4	79,390	1.53	81,580	1.55	87,450	1.73
8	82,060	1.51	76,490	1.59	81,280	1.74
12	81,480	1.52	71,590	1.55	80,410	1.61
16	82,350	1.52	65,260	1.60	59,610	1.69
20	83,010	1.35	69,660	1.39	59,770	1.59